ACS APPLIED MATERIALS & INTERFACES

RESEARCH ARTICLE

www.acsami.org

Modular "Click" Chemistry for Electrochemically and Photoelectrochemically Active Molecular Interfaces to Tin Oxide Surfaces

Michelle C. Benson, Rose E. Ruther, James B. Gerken, Matthew L. Rigsby, Lee M. Bishop, Yizheng Tan, Shannon S. Stahl, and Robert J. Hamers*

Department of Chemistry, University of Wisconsin-Madison, 1101 University Avenue Madison, Wisconsin 53706, United States

Supporting Information

ABSTRACT: We demonstrate the use of "click" chemistry to form electrochemically and photoelectrochemically active molecular interfaces to SnO_2 nanoparticle thin films. By using photochemical grafting to link a short-chain alcohol to the surface followed by conversion to a surface azide group, we enable use of the Cu(I)-catalyzed azide−alkyne [3 + 2] cycloaddition (CuAAC) reaction, a form of "click" chemistry, on metal oxide surfaces. Results are shown with three model compounds to test the surface chemistry and subsequent ability to achieve electrochemical and photoelectrochemical charge transfer. Surface-tethered ferrocene groups exhibit good electron-transfer characteristics with thermal rates estimated at >1000 s^{-1}. Time-resolved surface photovoltage measurements using a ruthenium terpyridyl coordination compound demonstrate photoelectron charge transfer on time scales of nanoseconds or less, limited by the laser pulse width. The results demonstrate that the CuAAC "click" reaction can be used to form electrochemically and photoelectrochemically active molecular interfaces to SnO_2 and other metal oxide semiconductors.

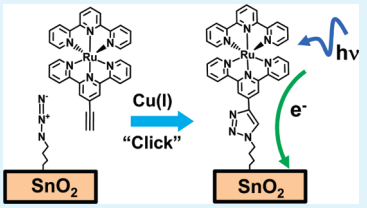

KEYWORDS: click chemistry, tin oxide, surface, electron transfer, metal oxide, surface functionalization

INTRODUCTION

Recent interest in hybrid organic−inorganic structures for applications such as low-cost solar cells[1−6] and photocatalysis[7−10] is placing increased emphasis on the development of optimized interfacial chemistries for linking molecular systems to metal oxide semiconductors. SnO_2, TiO_2, and related oxides are of interest because their semiconducting nature enhances charge separation at the molecule-semiconductor interface.[11,12] SnO_2 is of particular interest in applications such as dye-sensitized solar cells[13−23] because the conduction band of SnO_2 is lower in absolute energy than that of TiO_2 or ZnO, facilitating electron transfer from surface-attached molecules into SnO_2.[20] The larger bandgap (3.6 eV) of SnO_2 also reduces creation of photoexcited holes, which can degrade surface-attached dyes.[17,21] Finally, SnO_2 films exhibit electron mobilities on the order of 10 $cm^2\ V^{-1}\ s^{-1}$,[24,25] much higher than the values of ∼1×10^{-4} to 1×10^{-6} $cm^2\ V^{-1}\ s^{-1}$ typically obtained from nanocrystalline TiO_2 films.[26] High electron mobilities are advantageous because they enhance charge separation and lower the resistance of the films.

Previous studies have shown that molecules terminated with carboxylic acid,[18,27] phosphonic acid,[28−30] and silane groups[15,18] can be used to link molecules to SnO_2 surfaces. The one-step adsorption of highly functional molecules such as dyes or catalysts to metal oxides typically requires relatively difficult synthesis and purification steps en route to each of the derivatized compounds.[28,31] A more general approach to forming molecular interfaces to surfaces uses a bifunctional molecule that links to the surface using one functional group and leaves the second functional group exposed at the outermost surface; photochemically or or electrochemically active molecules can then be linked to the modified surface via this exposed functional group. A similar bifunctional-linker approach has been used to make electrochemically or photochemically active surfaces of materials including silicon,[32−34] diamond,[35,36] gold,[37,38] graphite,[37] and SnO_2.[18] In this two-step approach, surface attachment and compound synthesis chemistries thus become modular and orthogonal. A prior study using this approach with SnO_2 linked dyes to the surface via amide and thiol linkages.[18] Recent studies have shown that highly efficient reactions generically known as "click" reactions[39−41] provide a versatile route toward highly functional surfaces.[36−38,42] The Cu(I)-catalyzed azide−alkyne cycloaddition (CuAAC) reaction is of particular interest because studies on carbon surfaces have shown that the resulting triazole linkages are highly stable even under highly oxidizing conditions and support electron-transfer processes.[36,38,42,43]

Here, we present recent work investigating the use of the Cu(I)-catalyzed azide−alkyne cycloaddition (CuAAC) reaction[39−41] as a modular approach to fabrication of molecular interfaces to SnO_2. Our results show that by starting with a short linker molecule to produce a high density of surface azide groups separated slightly

Received: May 17, 2011
Accepted: July 18, 2011
Published: July 18, 2011

from the SnO_2 surface, it is possible to use the CuAAC reaction to link more complex molecular structures to the azide-modified SnO_2 surface. Ferrocene and a ruthenium terpyridyl complex were used as model systems to show that the resulting interfaces support both electrochemical and photoelectrochemical charge transfer.

EXPERIMENTAL SECTION

Synthesis of SnO_2 Nanoparticles and Preparation of SnO_2 Films. SnO_2 nanoparticles were synthesized following previously reported procedures, via hydrolysis of $SnCl_4$ under basic conditions followed by calcining.[44] In a typical reaction 2.22 mmol of $SnCl_4 \cdot 4H_2O$ and 50.0 mmol of NaOH were ball-milled for 15 s, followed by addition of 1.11 mmol NaCl and further milling for 30 s. The mixture was annealed at 400 °C for 2 h, washed with deionized water three times, then dried at 100 °C for 1 h. The resulting nanocrystalline SnO_2 powder was collected and analyzed using scanning electron microscopy (SEM) and X-ray diffraction (XRD) methods. Figure S1 in the Supporting Information shows a SEM image of the nanoparticles dispersed on a conducting substrate; the nanoparticles showed an average diameter of approximately 50 nm. Figure S2 in the Supporting Information shows X-ray diffraction (XRD) data for the nanoparticles demonstrating that they form the tetragonal (cassiterite) phase, the most common phase of SnO_2.[20] A limited number of experiments were also performed using purchased nanoparticles (Nanostructured and Amorphous Materials, Los Alamos, NM); a direct comparison of our synthesized nanoparticles with those purchased showed no significant differences between the particles we synthesized and those we purchased.

To enhance sensitivity for analytical measurements while avoiding transport and rinsing issues that can affect chemical reactions in highly porous films, we performed the experiments reported here using nanoparticle films that were sintered to form a nonporous film with surface texturing to provide enhanced surface area. This was achieved using a variation of a method commonly used for making porous films.[45] Typically, a 120 mg sample of SnO_2 was suspended in absolute ethanol via sonication. To the suspended mixture was mixed 335 mg of 10 wt % ethyl cellulose (46070, Sigma-Aldrich, Milwaukee, WI) in absolute ethanol (EtOH) with 260 mg of 10 wt % (in absolute EtOH) ethyl cellulose (46080, Sigma-Aldrich), and 484 mg of anhydrous terpineol (16406, Sigma-Aldrich) were added. The mixture was subjected to ultrasonication for 30 min and the solvent was removed using rotary evaporation. The paste was then screen-printed onto the desired substrate, and the screen-printed substrate with paste applied was sintered at 600 °C for 1 h, followed by one additional hour at 500 °C. This procedure yielded a highly textured, sintered film well suited for for further functionalization and analysis. Two types of substrates were used. All experiments were performed using substrates consisting of a thin film of fluorinated tin oxide (FTO) on glass (sheet resistance 15 Ω/sq, Hartford Glass, Hartford City, IN) because these substrates provide good electrical contact to the SnO_2 nanoparticle films and are transparent. As an additional control, duplicate XPS experiments were performed on some samples using substrates consisting of 100 nm Ti evaporated onto heavily doped Si wafers, thereby providing fluorine-free substrates. Experiments using the latter substrates provided a way to confirm that the XPS experiments (described below) probed the SnO_2 nanoparticle film and not the underlying substrate. Unless otherwise stated, all results shown here were obtained using sintered SnO_2 films fabricated on the fluorinated tin oxide substrates.

Figure S3 in the Supporting Information shows a representative SEM image after the nanoparticles were processed into a continuous film. SEM images of multiple samples showed that the SnO_2 films used were typically 700 nm to 1 μm in thickness. The sintered SnO_2 films have a highly textured surface but have a relatively low porosity. The highly textured nature of the SnO_2 surface provided higher surface area than a comparable planar film (estimated as approximately a 2-fold enhancement by visual inspection of the SEM images), thereby enhancing the sensitivity of the surface analytical measurements. We chose to use sintered films with a low porosity in studies presented here because this structure confined the liquid reactants to a thin layer near the outmost surface, thereby avoiding potential reactions with the underlying substrate, enhancing transport of reactants to the SnO_2 surface reaction sites, and facilitating proper rinsing of the SnO_2 films after reaction. These factors are important in making unambiguous distinction between species chemically bound to the SnO_2 surface and those physically adsorbed or trapped in the film via noncovalent interactions.

Molecular Reagents. We investigated the coupling of three different molecules to the SnO_2 surface. The compounds 4-(trifluoromethoxy)phenylacetylene (TFMPA) and ethynylferrocene were purchased commercially (Sigma-Aldrich, Milwaukee WI). We also prepared the $[Ru(tpy)(tpy')]^{2+}$ (tpy = 2,2′:6′,2″-terpyridyl), (tpy′=4-ethynyl-2,2′:6′,2″-terpyridyl) derivative bearing a pendant alkyne group; synthesis and characterization of this molecule has been described previously.[46] All other reagents were purchased from Sigma-Aldrich unless stated otherwise.

Fourier-Transform Infrared (FTIR) Measurements. Infrared spectra were collected using an FTIR spectrometer (Vertex 70, Bruker Optics, Billerica, MA) at a resolution of 4 cm^{-1}. FTIR spectra were collected in single-bounce external reflection mode using a variable angle specular reflectance accessory with a wire grid polarizer (VeeMAX II, Pike Technologies, Madison, WI). All reflection spectra were collected with p-polarized light at an incident angle of 50° from the surface normal. FTIR spectra of functionalized surfaces were measured using an unfunctionalized sample as the background. Residual baselines were removed to improve the clarity of the spectra. Baseline correction was achieved using a polynomial fit to remove sloping and/or curved background. A single polynomial was fit to each spectrum, taking care to avoid any regions containing peaks likely to be associated with surface species. The polynomial fits typically included the following regions: 3150−3250, 2700−2420, 2300−2175, 1890−1770, and 1670−1490 cm^{-1}. In each case, the experimental spectrum was fit to a polynomial using all points in the selected regions, and the resulting polynomial was then subtracted from the data. In general, fits were performed using several different polynomial orders in order to ensure that the spectral features observed were not sensitive to the precise details of the fitting procedure.

X-ray Photoelectron Spectroscopy (XPS). XPS data were obtained using a custom-built XPS system (Physical Electronics Inc., Eden Prairie, MN) consisting of a model 10−610 Al Kα source (1486.6 eV photon energy) with a Model 10−420 toroidal monochromator and a model 10−360 hemispherical analyzer with a 16-channel detector array; measurements were typically performed using a electron takeoff angle of 45°. Peak areas were calculated by fitting the raw data to Voigt functions after a Shirley baseline correction.[47,48] The Voigt function consists of a mixed Gaussian−Lorentzian of the form $f(x) = (A)/\{1+(m(E-E_0)^2)/(w^2)\}\exp\{(1-m)(\ln 2)(E-E_0)^2/(w^2)\}$.[48] In this equation, w is the peak width parameter, E_0 is the binding energy of the peak center, E is the binding energy, m is the mixing ratio ($m = 0$ for pure Gaussian, $m = 1$ for pure Lorentzian), and A is an amplitude coefficient. The spectra of each sample were shifted as necessary to make the primary C(1s) peak lie at a fixed energy of 284.4 eV; all other spectra for a given sample were shifted by the same amount.

Electrochemical Characterization. All electrochemical measurements were performed using an Autolab potentiostat (PGSTAT302N, Metrohm Autolab B.V., Utrecht, The Netherlands) using the SnO_2 samples as the working electrode, a Bioanalytical Systems (BASi, West Lafayette, IN) Ag/AgCl junctioned reference electrode, and a platinum wire counter-electrode. The aqueous Ag/AgCl reference electrode consisted of a silver wire immersed in a solution of 3 M NaCl.

Scheme 1. (a) Formation of Azide-Terminated SnO_2 Surface, and (b) Subsequent CuAAC Reaction with Organic Alkyne

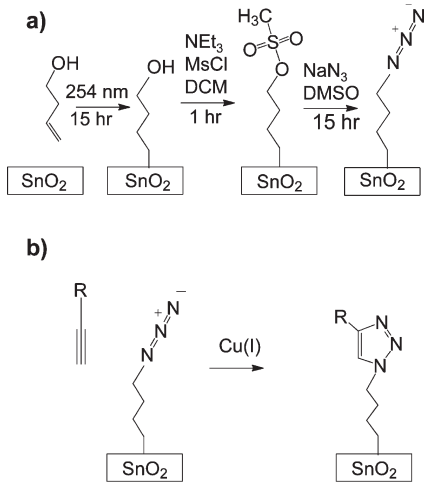

Optical Characterization. Absorption spectra were obtained on a UV−visible spectrophotometer (UV240PC, Shimadzu, Addison, IL). Excitation and emission spectra were measured on a spectrofluorimeter (Model K2, ISS, Champaign-Urbana IL).

Time-Resolved Surface Photovoltage (TR-SPV) Measurements. Time-resolved surface photovoltage measurements[49−51] were performed using a custom-made cell holder in which a pickup electrode was held 25 μm away from the sample surface. The entire cell was sealed inside an argon glovebox. The sample was illuminated with short pulses (<3 ns, 600 μJ/pulse) from a tunable laser system (NT340, Ekspla, Inc., Vilnius, Lithuania); the resulting injection of electrons from the surface into the bulk induced transient changes in the potential, and these changes were measured at the pickup electrode. The sense electrode signal was amplified using a fast amplifer (Model TA2000B-3, FAST ComTec GmbH, Oberhaching/München, Germany) with a 50 Ω input and output impedances, 1.5 GHz bandwidth, and 40x voltage gain. The amplified output was recorded on a sampling digital oscilloscope (Model DSO5054A, Agilent, Inc., Santa Clara, CA).

RESULTS

Preparation of Azide-Functionalized SnO_2 Surfaces. A key step in enabling the CuAAC reaction on metal oxides is forming azide or alkyne groups on the surfaces. We chose to focus on preparing azide-modified SnO_2 surfaces both because it is easier to synthesize and store molecules bearing alkyne groups than molecules with azide groups (which are often explosive), and because alkyne-modified molecules are generally easier to obtain commercially. We prepared azide-functionalized SnO_2 nanocrystalline thin films via the three-step process shown in Scheme 1a.

The first step involved photochemical grafting of 3-buten-1-ol to the surface using 254 nm ultraviolet light (~10 mW/cm^2, 15 h) to give a high density of surface alcohol groups that are slightly removed from the bare SnO_2 surface. Photochemical grafting of alkenes has been shown to yield highly stable molecular layers on surfaces of TiO_2[52] and other oxides.[53] Although the grafting mechanism has not been fully elucidated, studies to date suggest that photoexcited surface −OH groups act as hole traps that facilitate nucleophilic attack by the organic alkene group to link the molecules to the surface.[52,54] We then converted the surface alcohol groups to methanesulfonyl ("mesyl") groups using methanesulfonyl chloride (MsCl) with triethylamine (NEt_3) in dichloromethane (DCM).

Scheme 2. Reaction of TFMPA with Azide-Modified Surface

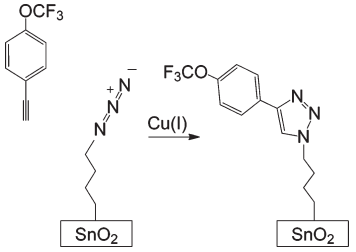

The surface-bound mesyl groups were replaced by azide groups by treatment with NaN_3. (***Warning**: sodium azide is highly toxic and should be used with caution.*) Detailed procedures for these steps are given in the Supporting Information, along with FTIR spectra showing the sample after photochemical grafting of 3-butene-1-ol, after the mesylation step, and after conversion to the azide. The molecules of interest were then coupled to the azide-terminated surfaces via the CuAAC reaction[39,41] as depicted in Scheme 1b. Here we report results using three different "R" groups to demonstrate successful "click" chemistry and to explore its application to systems involving electrochemical and photoelectrochemical electron transfer.

Grafting of TFMPA to SnO_2 Surfaces. Because the use of "click" chemistry to functionalize metal oxides has not been demonstrated previously, we first investigated the formation of the azide-terminated surfaces and demonstrated their reactivity by using a compound that facilitates analytical characterization via XPS and FTIR spectroscopy. For this purpose we used the compound 4-(trifluoromethoxy)phenylacetylene (TFMPA), which we linked to SnO_2 surfaces as depicted in Scheme 2.

To graft TFMPA to the surface, the azide-modified SnO_2 thin film was submerged in a solution containing 0.5 mM Cu(II)-(tris-(benzyltriazolyl-methyl)amine)$(BF_4)_2$ (henceforth referred to as TBTA), 1.0 mM of TFMPA, and 25 mM of sodium ascorbate in 3:1 (v:v) DMSO:H_2O for 17 h at room temperature. The samples were then rinsed sequentially with deionized H_2O, $CHCl_3$, and isopropyl alcohol (IPA). Experiments performed using shorter coupling times of 90 min and 5 h showed incomplete reaction, while the reaction was complete at 14 h. Reaction times of >14 h were used in all subsequent experiments. Similar reaction times have been used in previous studies of CuAAC reactions on azide-terminated silicon[33] and diamond[35] surfaces. The longer reaction times relative to those typically reported for reactions in solution likely reflects the increased steric constraints at surface-bound functional groups.

Figure 1 shows infrared spectra of an azide-modified SnO_2 surface, of an azide-modified SnO_2 surface after the CuAAC reaction with TFMPA, and of neat TFMPA. Figure 1a shows the entire region of interest, while Figure 1b is an enlarged view of the 1100−1600 cm^{-1} region. The spectrum of neat TFMPA is dominated by three C−F modes at 1165, 1211, and 1255 cm^{-1} and a sharp mode at 1205 cm^{-1}. On the basis of a previous normal-mode analysis of a closely related molecule, trifluoromethoxybenzene, we attribute the 1205 cm^{-1} peak to an aromatic ring mode.[55] The azide-modified SnO_2 surface exhibits a very sharp peak at 2096 cm^{-1} that is characteristic of the symmetric stretch of the azide group, along with C−H modes at 2914 and 2860 cm^{-1} from the 3-buten-1-ol molecule. In

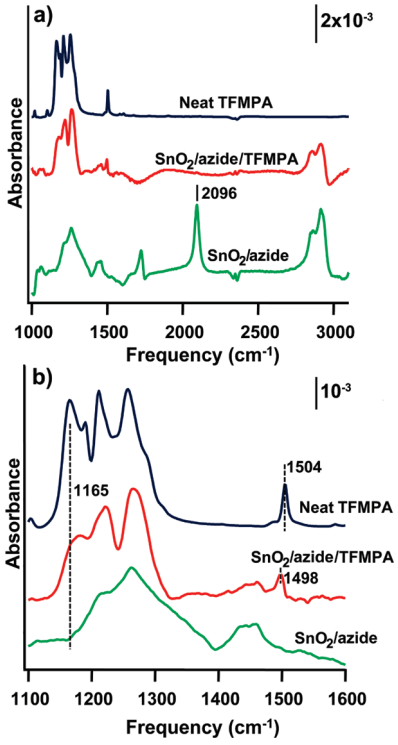

Figure 1. (a) FTIR spectra of SnO_2 film after functionalization with azide and after complete CuAAC reaction with TFMPA. Also shown is the spectrum of neat TFMPA. (b) Same as (a), showing an enlarged view of the 1100−1600 cm^{-1} range. The spectrum of neat TFMPA was scaled arbitrarily to facilitate comparison with the surface spectra. Spectra were shifted vertically for comparison.

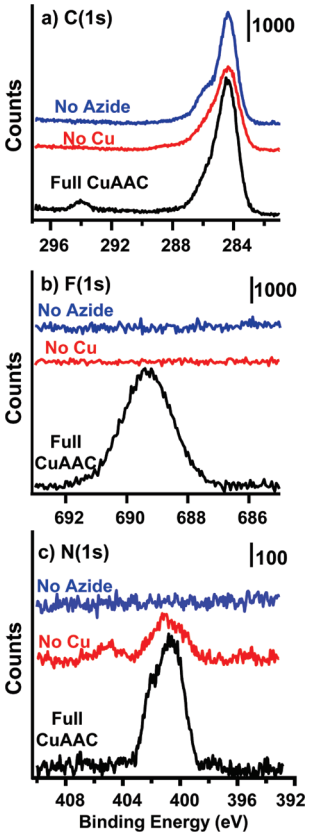

Figure 2. XPS spectra of SnO_2 sample after complete CuAAC reaction with TFMPA, and those of control samples that underwent the entire reaction sequence except for eliminating the mesylation/azidization steps ("No azide") or eliminating Cu during the CuAAC reaction ("No Cu"). (a) C(1s) region, (b) F(1s) region, and (c) N(1s) region.

addition, a broadened peak near 1261 cm^{-1} and a smaller peak near 1444 cm^{-1} arise from the alkyl chains of the butenol and lattice vibrations of SnO_2. Finally, a sharp peak at 1724 cm^{-1} is observed; this peak likely arises from the C═O stretch of adsorbed CO_2.[56]

Exposure of the azide-modified sample to TFMPA under the CuAAC conditions induces several important changes. The most pronounced change is the disappearance of the azide peak at 2096 cm^{-1}. The CuAAC-reacted sample also shows a peak at 1498 cm^{-1}; neat TFMPA shows a similar peak shifted at 1504 cm^{-1}.[55] Finally, the CuAAC sample shows a triplet of peaks at 1165, 1220, and 1265 cm^{-1}. These peaks are a clear superposition of the triplet of C−F peaks from TFMPA (with small shifts from the frequencies observed for neat TFMPA) and the broad 1150−1400 cm^{-1} feature of the azide-modified SnO_2 surface; the presence of the CF_3 group on the CuAAC-reacted sample is observed most clearly through the presence of the new 1165 cm^{-1} mode after the reaction.

XPS was used to further verify successful CuAAC reaction. Figure 2 shows the C(1s), F(1s), and N(1s) regions of an azide-modified sample that was reacted with TFMPA in the presence of the Cu(I) catalyst. Also shown are results from two control samples. One control sample ("No Cu") was carried through the entire procedure depicted in Schemes 1a and 2, except the Cu catalyst was left out during the final step. A second control sample ("No azide") was carried through the complete procedure except the mesylation/azidation sequence of Scheme 1a was eliminated. If the reactions proceed as depicted in Schemes 1 and 2, the "No azide" control should correspond to the alcohol-terminated surface, whereas the "No Cu" control should correspond to the azide-terminated surface.

The "Full CuAAC" sample shows a single F(1s) peak at 689.3 eV from the $-CF_3$ group of TFMPA. The C(1s) spectrum shows a main peak at 284.4 eV, a shoulder at ∼285.5 eV, and an isolated peak at 294.0 eV. The peak at 284.4 corresponds to nonoxidized carbon from the alkyl chain of the initial butenol layer and from the carbon atoms in the aromatic ring of TFMPA. The peak at 294.0 eV arises from C atoms in the CF_3 group of TFMPA, while the small shoulder at ∼285.5 eV is consistent with C atoms adjacent to either N or O atoms, which are both electron-withdrawing. Finally, the "Full CuAAC" sample shows two overlapping N(1s) peaks at 399.6 and 401.1 eV. The latter two peaks are very similar to those observed in previous CuAAC reactions on surfaces[36,43] and correspond to the N atoms in the triazole ring. Thus, the "Full CuAAC" spectrum is fully consistent with the spectrum expected from the reaction depicted in Scheme 2.

The coverage can be roughly estimated from the F(1s) and Sn(3d) peak areas. Using an electron escape depth of ∼2 nm in SnO_2[57] and atomic sensitivity factors of 4.1 for the Sn ($3d_{5/2}$) peak and 1.0 for F(1s)[58] yields an coverage of $\sim 1.7 \times 10^{15}$ TFMPA molecules/cm^2 in the planar-sample limit. However, this value is larger than the true molecular coverage because the textured nature of the film surface increases the effective surface area (and consequently the number of $-CF_3$ groups within the sampling area relative to the number of Sn atoms detected.

Scheme 3. Reaction of Ethynylferrocene with Azide-Modified SnO_2 Surface via CuAAC Reaction

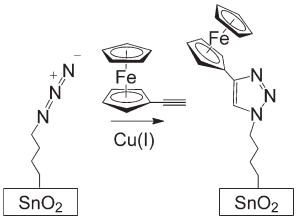

Accurate determination of molecular coverage would require detailed modeling of electron emission and scattering in the nanoparticle film, but simple geometric arguments indicate that the geometric corrections have a magnitude of approximately a factor of 2.[52] Thus, we estimate the true TFMPA coverage is on the order of 5×10^{14} to 1×10^{15} molecules/cm^2. Although the molecular coverage cannot be determined exactly, the values obtained are high and indicate that the molecules achieve dense packing on the surface.

Further confirmation that the surface grafting took place via the CuAAC reaction comes from the control samples. The spectrum of the "No Cu" control sample shows no detectable fluorine and a more complex N(1s) structure consisting of two peaks at 404.3 and 400.1 eV. The peak at 404.3 eV has a binding energy significantly higher than most N-containing compounds and is characteristic of the central N atom of the azido group, which has a formal positive charge (see Scheme 1a).[59] The presence of this peak on the "No Cu" control but not on the "Full CuAAC" sample is strong evidence for reaction of the azide group with the alkyne group of TFMPA to form the triazole ring.[36,43] The spectrum of the "No azide" sample shows no detectable F(1s) or N(1s) intensity but shows two C(1s) peaks: a main peak at 284.4 eV and a shoulder at 285.9 eV. The 284.4 eV peak arises from the alkyl chains while the 285.9 eV peak is consistent with that expected from C atoms of alcohol groups. These control experiments establish several important facts. First, the absence of any F(1s) signal on the two control samples shows that there is no significant nonspecific binding of TFMPA to the surface. Second, they show that the CuAAC reaction requires the Cu(I) to catalyze the cycloaddition between the azide terminated nanocrystalline thin-film SnO_2 and TFMPA. The XPS data are fully consistent with the FTIR data, and both XPS and FTIR results confirm that the CuAAC reaction proceeds as depicted in Scheme 2.

Formation and Characterization of Ferrocene-Modified SnO_2 Surfaces via CuAAC Reaction. The XPS and FTIR data above establish the successful use of CuAAC chemistry to link model compounds to the surface of SnO_2. To test the generality of the method and reaction conditions, we tested the ability to make surface adducts with molecules that are expected to exhibit charge-transfer processes under electrochemical and photoelectrochemical conditions. Ferrocene is useful as a model system for testing electron transfer because the CuAAC reaction has been used previously to form ferrocene-terminated layers on carbon-based materials[37,43] and on self-assembled monolayers on gold.[38,42] Scheme 3 depicts the binding of ethynylferrocene to the SnO_2 surface. In this case, the azide-modified SnO_2 thin-films were immersed in a solution containing 3.8 mM ethynylferrocene, 8.0 mM sodium ascorbate, 0.4 mM $Cu(BF_4)_2$, and 0.1 mL of triethylamine in 3:1 (v:v) DMSO:H_2O. The reaction was carried out at room temperature for 17 h, and the sample was then rinsed sequentially with MeOH, $CHCl_3$, and IPA.

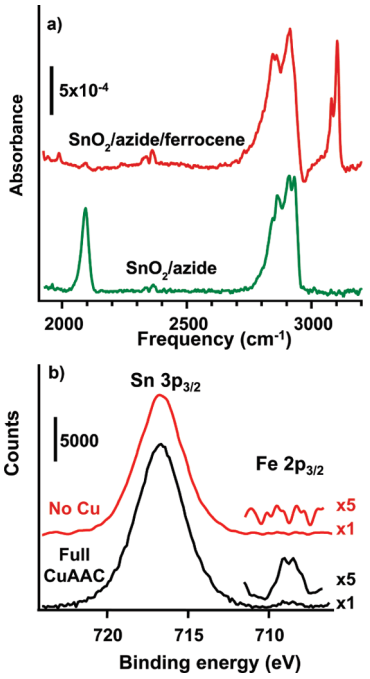

Figure 3. FTIR and XPS characterization of ferrocene-modified SnO_2. (a) Infrared spectra of azide-modified SnO_2 thin film before and after CuAAC reaction with ethynylferrocene. (b) XPS spectra of sample exposed to full CuAAC condition, and control sample without Cu catalyst ("No Cu").

Figure 3a shows FTIR spectra of the azide-modified SnO_2 surface before and after the CuAAC reaction with ethynylferrocene. The azide-modified surface shows the characteristic 2100 cm^{-1} azide peak. After reaction with ethynylferrocene the 2100 cm^{-1} peak decreases almost completely, and a new sharp peak at 3103 cm^{-1} appears. The latter matches very well the 3106 cm^{-1} peak associated with the aromatic C−H modes of ferrocene vapor.[53] The nearly complete elimination of the azide stretch upon reaction with ethynylferrocene suggests that the CuAAC reaction is highly efficient, and that the ferrocene groups can pack sufficiently close together to allow the vast majority of exposed azide groups to react with ethynylferrocene.

XPS spectra were also obtained of the ferrocene-modified surface. The most clear signature of surface-bound ferrocene is the appearance of an Fe ($2p_{3/2}$) peak in the XPS spectra near 709 eV, as shown in Figure 3b. This peak is weak and riding on the side of the much larger Sn ($3p_{3/2}$) peak, but it is clearly visible on the sample exposed to the full CuAAC conditions and is absent on the control sample ("No Cu") that was processed similarly but without any Cu catalyst used. Taken together the XPS and FTIR data again strongly support the successful grafting of ferrocene groups to the SnO_2 surface.

Electron-Transfer Properties of Ferrocene-Modified Layers. To determine if the ferrocene groups linked to SnO_2 are electrochemically active, we conducted experiments using cyclic voltammetry. Figure 4 shows representative cyclic voltammograms (CVs) of ferrocene-modified SnO_2 surfaces measured at sweep rates of 0.3 V/s, 1 V/s, 3 V/s, and 10 V/s along with a control sample. The "no azide" control sample consisted of an identical sample that was modified with butenol and exposed to the

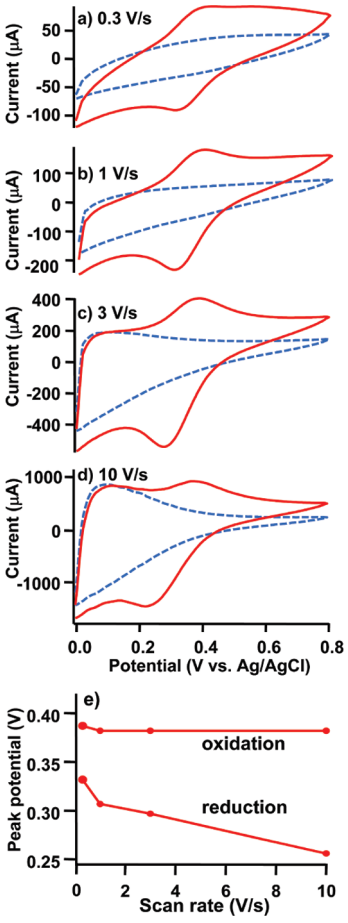

Figure 4. Cyclic voltammograms of SnO_2 sample after complete CuAAC reaction to graft ethynylferrocene (solid lines), and "no azide" control sample as described in text (dashed lines). Results are shown at scan rates of (a) 0.3, (b) 1, (c) 3, and (d) 10 V/s. Panel e) shows the peak potentials of the oxidation and reduction waves at the different scan rates for the ferrocene-modified sample .

complete "click" grafting solution (including ferrocene), but was not exposed to the mesylation/azidation sequence of Scheme 1a.

Because previous studies have shown that the ferrocenium cation is rapidly degraded by nucleophiles such as OH^- and Cl^-,[60] we used 1 M aqueous $HClO_4$ as the supporting electrolyte. For a perfect redox-active monolayer on a metallic surface, the splitting between oxidized and reduced waves should approach zero at infinitely slow scan rate,[61,62] and the background from the (nonfunctionalized) electrode should be a simple trapezoid arising from the Helmholtz capacitance of the interface and uncompensated solution resistance. With semiconductors; however, the semiconductor space-charge layer and surface defects introduce additional resistance and capacitance components. These effects are particularly important for nanocrystalline semiconductor films because they have very high density of surface states.[63,64]

The CVs we obtain on the "no azide" control sample are similar to those reported previously on bare nanocrystalline films of SnO_2[65] and TiO_2.[64] Those studies showed that nanocrystalline SnO_2 and TiO_2 films have chloride impurities[65] and bulk oxygen vacancy defects that create a band of unoccupied states in the bandgap. The gap states have a distribution of energies extending from the conduction band edge into the bandgap, thereby giving rise to an interfacial capacitance that is dependent on sample potential and scan rate.[64] The general shape of the background scans is well-described by these models[65] and will not be considered further here. For our studies the important observation is that "no azide" control sample does not show any peaks that can be attributed to oxidation or reduction of ferrocene. Because this sample was exposed to ethynylferrocene (but lacked the azide group), the absence of ferrocene-related redox features confirms that the binding of ferrocene to the surface requires the presence of the surface azide group.

In contrast to the butenol-modified surfaces, the azide-modified SnO_2 surfaces that were exposed to the full CuAAC conditions clearly show both oxidation and reduction peaks at ~0.3−0.4 V vs Ag/AgCl from the surface-bound ferrocene groups, close to the values previously reported for ferrocene self-assembled monolayers on gold.[66] On SnO_2, these peaks are riding on top of a voltage-dependent background that is similar to that observed on the butenol-modified sample.

Further insights can be gleaned from analysis of the potentials at which the oxidation and reduction waves reach their maxima, by subtracting the capacitive background from the oxidation and reduction waves at each scan rate. Figure 4e summarizes the potentials at which the oxidation and reaction peaks reached their maximum current. In contrast to the limit of zero splitting expected for a perfectly reversible system, ferrocene on SnO_2 shows a splitting between oxidation and reduction waves of ~50 mV even at the lowest scan rates. This nonzero splitting indicates that the electron transfer is not fully reversible. At higher scan rates the splitting becomes larger, but in an asymmetric manner: the peak potential for the oxidation wave remains nearly constant while the potential of the reduction wave changes significantly with scan rate. A lower bound on the standard electrochemical charge-transfer rate k^0_{ct} can be estimated from the peak-to-peak splitting, ΔE_{pp}, and rate, R, as $k^0_{ct} = R/\Delta E_{pp}$. This value is a lower bound because it neglects other charge transfer processes that can limit the rate at which the surface potential changes, such as space-charge effects and/or charging of surface states. The 50 mV change in ΔE_{pp} as the scan rate is increased from 0 to 10 V/s in Figure 4d yields a lower limit of $k^0_{ct} > 1000\ s^{-1}$. The peak splitting we observe here is smaller than that observed in previous work linking ferrocene to SnO_2 and TiO_2 via a phosphonic acid linkage, where a peak-to-peak splitting of ~400 mV was observed on SnO_2 and 390 mV on TiO_2.[30] The small value we observe here suggests that the CuAAC reaction substantially improves the electron communication between ferrocene and the underlying oxide surface compared with the approach employed previously. In repeated cycling, the cyclic voltammograms were extremely stable for more than 100 repeated cycles but eventually degraded, likely to the inherent instability of SnO_2 in acidic conditions. Cyclic voltammograms obtained after 1 cycle and after 100 cycles are shown in the Supporting Information.

Integration of the oxidation peak yields a total integrated charge of 2.2×10^{-5} coulombs. Using the projected sample area, this corresponds to 5×10^{14} redox active ferrocene groups/cm^2. This value is at the lower end of the range of 5×10^{14} to 1×10^{15} molecules/cm^2 estiamted from XPS studies of TFMPA, consistent with the slightly larger size of the ferrocene molecule.

Photoelectrochemically Active Charge-Transfer Complex. The above data show that electron transfer under quasi-reversible conditions typical of electrochemical reactions can occur. To test whether the use of the CuAAC chemistry would allow surface-tethered molecules in excited electronic states to transfer

Scheme 4. CuAAC Reaction Linking $[Ru(tpy)(tpy')]^{2+}$ to Azide-Modified SnO_2 Surface

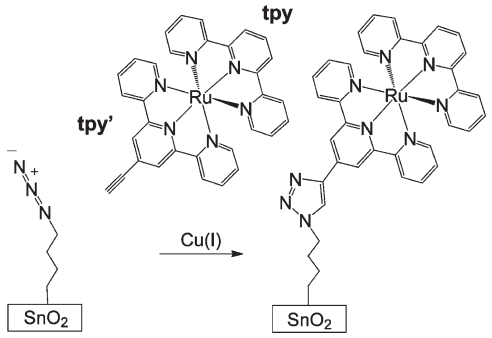

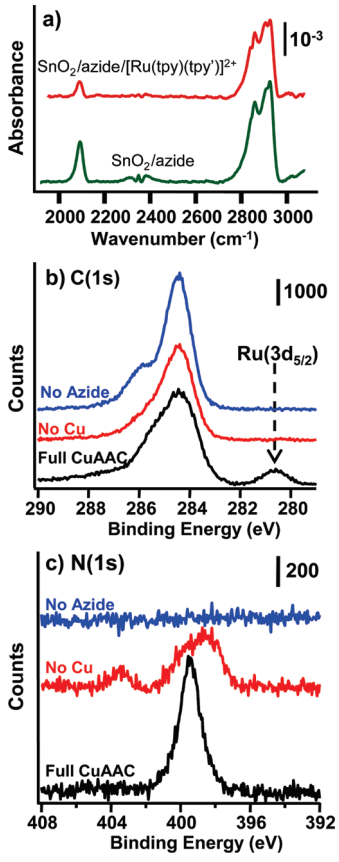

Figure 5. Characterization of CuAAC reaction of $[Ru(tpy)(tpy')]^{2+}$ with the SnO_2 surface. (a) FTIR spectra after modification with the azide group and after full CuAAC reaction with $[Ru(tpy)(tpy')]^{2+}$. (b, c) C(1s) and N(1s) XPS data showing the C(1s) and $Ru(3d_{5/2})$ peaks for $[Ru(tpy)(tpy')]^{2+}$and control samples.

electrons into the SnO_2 conduction band on faster time scales, we used time-resolved surface photovoltage measurements to probe the photoinitiated injection of electrons from a Ru-based coordination complex into the SnO_2 nanocrystalline film. For these experiments, we used the alkyne-modified coordination complex $[Ru(tpy)(tpy')]^{2+}$ shown in Scheme 4.

Ruthenium coordination complexes have attracted wide attention for their unique photophysical properties.[10,67] The $[Ru(tpy)(tpy')]^{2+}$ complex in Scheme 4 was chosen because in

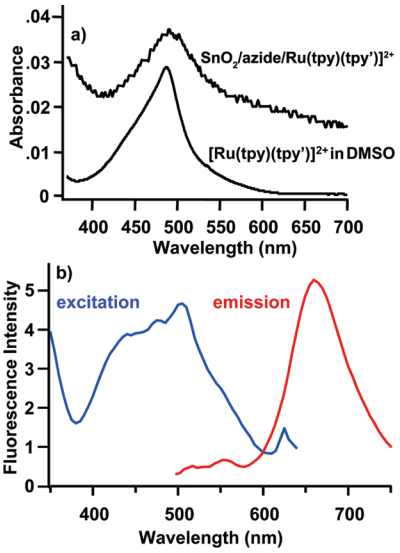

Figure 6. (a) Absorption spectrum of $[Ru(tpy)(tpy')]^{2+}$ grafted onto SnO_2 surface and solution-phase absorption spectrum of $[Ru(tpy)(tpy')]^{2+}$ in DMSO. The spectra have been scaled individually and shifted vertically for clarity. b) Fluorescence emission spectrum (480 nm excitation) and fluorescence excitation spectrum (680 nm emission) of $[Ru(tpy)(tpy')]^{2+}$ in DMSO.

recent studies[36] we showed that this coordination complex exhibits extraordinary chemical and electrochemical stability when linked to diamond surfaces via a similar CuAAC reaction, and because a phosphonic acid-modified compound has been investigated previously on TiO_2 and SnO_2.[28] Here, we linked this complex to SnO_2 surfaces by immersing the azide terminated SnO_2 in a solution of 100 μM $[Ru(tpy)(tpy')]^{2+}$, 0.8 mM CuTBTA, and 15 mM sodium ascorbate in 3:1 (v:v) DMSO: H_2O for 18 h at room temperature. The samples were rinsed sequentially with MeOH, $CHCl_3$, and IPA.

FTIR (Figure 5a) and XPS data (Figure 5b, c) provide evidence for functionalization of the azide-modified SnO_2 surface with the $[Ru(tpy)(tpy')]^{2+}$ complex. The FTIR data obtained before and after the reaction are qualitatively similar to those observed with TFMPA and ethynylferrocene. However, reduction of the peak intensity at 2100 cm^{-1} (surface azide peak) after the CuAAC reaction with $[Ru(tpy)(tpy')]^{2+}$ is less complete than what was observed with TFMPA or ethynylferrocene. This observation suggests that steric interactions limit the efficiency of the surface CuAAC reaction. In the XPS data, the $Ru(3d_{5/2})$ peak is close to the primary C(1s) peak (Figure 5b); the $3d_{3/2}$ spin−orbit component should be 2/3 the intensity of the $3d_{5/2}$ component and should lie under the C(1s) peaks. The N(1s) peaks (Figure 5c) again show the characteristic changes expected from the azide functionalization step and subsequent CuAAC reaction.

Figure 6 shows optical absorption spectra of the $[Ru(tpy)(tpy')]^{2+}$ complex in DMSO, and a measurement made in transmission mode of the complex linked to the SnO_2 surfaces. The spectrum of $[Ru(tpy)(tpy')]^{2+}$ in DMSO has a maximum at 487 nm and appears similar to that reported previously for the unmodified $[Ru(tpy)_2]^{2+}$ in acetone[68] and in acetonitrile.[69] The spectrum of the $[Ru(tpy)(tpy')]^{2+}$ bound to the surface appears similar to the solution-phase spectrum, although slightly broadened and red-shifted, with the absorption maximum at 496 nm. This shift results from additional delocalization of the electrons onto the triazole ring

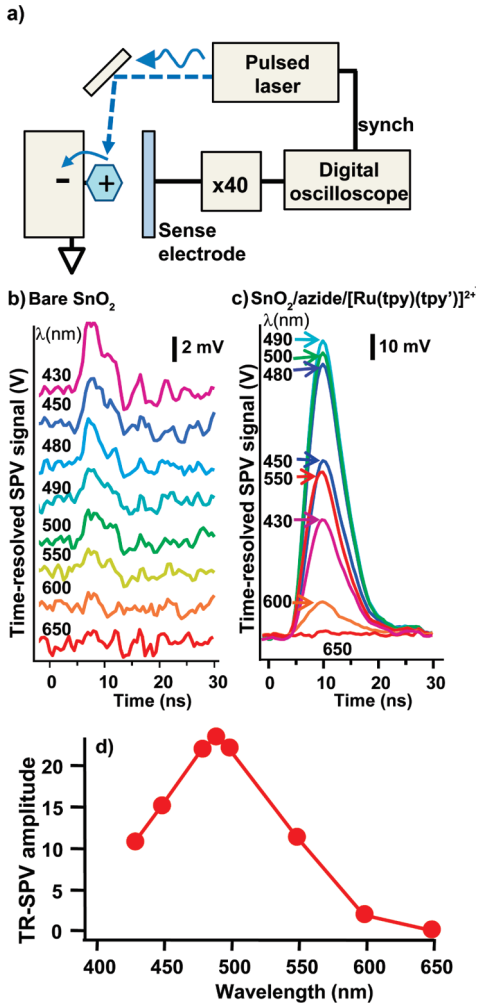

Figure 7. Time-resolved surface photovoltage measurements of $[Ru(tpy)(tpy')]^{2+}$ on SnO_2. (a) Schematic illustration of apparatus. (b) TR-SPV data from bare SnO_2 at different wavelength (indicated in nm). (c) TR-SPV data from SnO_2 after grafting of $[Ru(tpy)(tpy')]^{2+}$ complex at different wavelengths (nm). (d) TR-SPV signal amplitude normalized by photon energy for $[Ru(tpy)(tpy')]^{2+}$ linked to SnO_2.

and is indicative of covalent bond formation. The excitation spectrum of $[Ru(tpy)(tpy')]^{2+}$ in DMSO at an emission wavelength of 680 nm shows a more complex spectrum, with a broad but structured peak at 505 nm, and additional peaks at 290 and 405 nm. The emission spectrum with excitation at 480 nm shows a maximum at 660 nm.

To characterize the charge injection of the $[Ru(tpy)(tpy')]^{2+}$ complex into the nanocrystalline SnO_2 thin-film conduction band, time-resolved surface photovoltage (TR-SPV) measurements were performed. Figure 7a depicts the TR-SPV apparatus. Figure 7b and Figure 7c show the resulting TR-SPV transients measured at different wavelengths for the bare SnO_2 surface (Figure 7b) and for $[Ru(tpy)(tpy')]^{2+}$ bound to the SnO_2 surface (Figure 7c). A constant energy of 600 μJ/pulse, 20 Hz pulse rate was used.

The bare SnO_2 surface (Figure 7b) shows no significant response in most of the visible region, although there is a small response at the shortest wavelengths. The $[Ru(tpy)(tpy')]^{2+}/SnO_2$ sample clearly generates a much larger transient SPV response (note the different vertical scales for Figure 7b,c). The response from the $[Ru(tpy)(tpy')]^{2+}/SnO_2$ sample reaches a maximum at 490 nm, close to where the absorption spectrum (Figure 6a) and fluorescence excitation spectrum (Figure 6b) exhibit maxima. The positive sign of the transients corresponds to injection of electrons from the molecule into the SnO_2 surface, which leaves the surface with a transient positive charge that is then detected via the sense electrode. The time-resolved signal shows a fast rise and an almost equally fast fall time, both corresponding to the ~3 ns width of the incident laser pulse. Because the rapid rise and decay are close to the bandwidth limits of the detection electronics, it is not possible to determine precise electron injection kinetics. However, the results demonstrate that optical excitation does induce significant charge transfer and that measurable charge transfer takes place on time scales of ~3 ns or less. The parent $Ru(tpy)_2^{2+}$ complex has an excited state lifetime of 250 ps at room temperature.[70]

Figure 7d shows normalized peak intensities vs wavelength, in which the peak amplitudes from Figure 7c have been normalized to represent the SPV generated per incident photon. This wavelength dependence appears similar to that of the UV−visible absorption spectrum in Figure 6, suggesting that all wavelengths capable of being absorbed are also able to inject electrons from the molecule into the SnO_2.

DISCUSSION

The above results demonstrate that photochemical grafting combined with the use of the CuAAC "click" reaction provides a versatile method to interface electrochemically and photochemically active molecules with SnO_2. It is reasonable to expect that this methods will be suitable to functionalize other metal-oxide semiconductor surfaces. The ability to transfer charge across molecular interfaces is central to the use of molecular adducts in applications such as photovoltaic devices and photocatalysis. Our results suggest that the methods described here may be promising for these and other emerging applications.

Our approach to functionalization involves the use of a short molecular linker (3-buten-1-ol) that provides a high density of surface alcohol groups that are slightly removed from the surface. By using a short spacer to move the −OH groups slightly away from the metal oxide surface we enable a wide range of organic chemistry reactions, such as the CuAAC reaction, to be used in subsequent transformations. This approach enables the surface-attachment chemistry to be optimized independently of the synthesis of redox- and photoactive molecular species.

One potentially adverse effect of this two-step chemistry is that the use of a molecular tether reduces the direct electronic coupling between the appended electron-injector groups and the metal oxide surfaces. For optimum electron transfer it might be desirable to link molecules to the surface using completely conjugated linkages. Recent studies on metals,[71−73] carbon nanostructures,[43,74] and conductive diamond;[36] however, have shown that electron transfer in disordered molecular systems can be surprisingly facile, even when alkyl chains and/or other nonconductive groups are included in the molecular chains. This enhanced electron transfer has been attributed to the increased conformational flexibility of loosely tethered molecules, which allows a closer approach of the molecule to the underlying substrate than would be the case for a densely packed self-assembled monolayer.[36,43,71−75] This property is further supported by previous studies of electron transfer in proteins[76] and in DNA layers on surfaces.[71,72,75]

Although extraction of quantitative rates from the ferrocene/SnO_2 data is complicated by the convolution of electron transfer and charge trapping/detrapping processes in SnO_2 gap states, our data with ferrocene imply that thermal electron transfer takes place with a standard rate constant of >1000 s^{-1}, and our data for $[Ru(tpy)(tpy')]^{2+}$ indicate that photoexcited electron transfer can take place on time scales of 3 ns or less from excited electronic states. Thus, we conclude that the use of "click" chemistry as outlined here can be used as a way to link a diverse range of electrochemically and photoelectrochemically active groups to metal oxide surfaces. Additional studies will be required to fully characterize the rates and mechanisms of electron transfer.

CONCLUSIONS

Our results demonstrate a modular approach to the functionalization of metal oxide surfaces to yield electrochemically and photoelectrochemically active surfaces. Photochemical grafting of a short molecular layer provides a convenient means to produce a high density of alcohol groups slightly separated from the highly ionic (and reactive) metal oxide surface. Therefore, subsequent steps, including conversion of surface −OH groups to surface azides, can be carried out without undue concern about the behavior of the underlying metal oxide. These steps then allow the Cu(I)-catalyzed azide−alkyne [3 + 2] cycloaddition "click" reaction to be carried out as a modular approach to form electrochemically and photoelectrochemically active metal oxide surfaces, demonstrated here through the model systems of ethynylferrocene and $[Ru(tpy)(tpy')]^{2+}$. Although alkyl chains such as the short 3-buten-1-ol as the initial functionalization layer are often considered to be insulating, our results show that surface-tethered organometallic and coordination compounds such as ferrocene and $[Ru(tpy)(tpy')]^{2+}$ can undergo facile electron transfer to the metal oxides. Our results suggest that the methods employed herein provide versatile and convenient pathways toward the formation of hybrid interfaces of metal oxides with organic molecules for potential applications in renewable energy.

ASSOCIATED CONTENT

Supporting Information. SEM images of SnO_2 nanoparticles and nanoparticle sintered films; X-ray diffraction data of synthesized SnO_2 nanoparticles. FTIR spectra of SnO_2 film at successive stages of functionalization; cyclic voltammograms of ferrocene-modified SnO_2. This material is available free of charge via the Internet at http://pubs.acs.org/.

AUTHOR INFORMATION

Corresponding Author
*E-mail: rjhamers@wisc.edu.

ACKNOWLEDGMENT

This work was supported by the U.S. Department of Energy Office of Basic Energy Sciences Grant DE-FG02-09ER16122 (R.J.H.). Development and synthesis of the $Ru[(tpy)(tpy')]^{2+}$ coordination complex was supported by the National Science Foundation Grant CHE-0802907 (S.S.S.).

REFERENCES

(1) Grätzel, M. *J. Photochem. Photobiol., C* **2003**, *4*, 145.
(2) O'Regan, B.; Grätzel, M. *Nature* **1991**, *353*, 737.
(3) Argazzi, R.; Bignozzi, C. A.; Heimer, T. A.; Castellano, F. N.; Meyer, G. J. *Inorg. Chem.* **1994**, *33*, 5741.
(4) Bouclé, J.; Ravirajan, P.; Nelson, J. *J. Mater. Chem.* **2007**, *17*, 3141.
(5) Kim, J. Y.; Kim, S. H.; Lee, H.-H.; Lee, K.; Ma, W. L.; Gong, X.; Heeger, A. J. *Adv. Mater.* **2006**, *18*, 572.
(6) Haick, H.; Hurley, P. T.; Hochbaum, A. I.; Yang, P.; Lewis, N. S. *J. Am. Chem. Soc.* **2006**, *128*, 8990.
(7) Chen, Z. F.; Concepcion, J. J.; Hull, J. F.; Hoertz, P. G.; Meyer, T. J. *Dalton Trans.* **2010**, *39*, 6950.
(8) Chen, Z. F.; Concepcion, J. J.; Jurss, J. W.; Meyer, T. J. *J. Am. Chem. Soc.* **2009**, *131*, 15580.
(9) Chen, Z. F.; Concepcion, J. J.; Luo, H. L.; Hull, J. F.; Paul, A.; Meyer, T. J. *J. Am. Chem. Soc.* **2010**, *132*, 17670.
(10) Ischay, M. A.; Anzovino, M. E.; Du, J.; Yoon, T. P. *J. Am. Chem. Soc.* **2008**, *130*, 12886.
(11) Woodhouse, M.; Parkinson, B. A. *Chem. Soc. Rev.* **2009**, *38*, 197.
(12) McNamara, W. R.; Milot, R. L.; Song, H. E.; Snoeberger, R. C., III; Batista, V. S.; Schmuttenmaer, C. A.; Brudvig, G. W.; Crabtree, R. H. *Energy Environ. Sci.* **2010**, *3*, 917.
(13) Gubbala, S.; Russell, H. B.; Shah, H.; Deb, B.; Jasinski, J.; Rypkema, H.; Sunkara, M. K. *Energy Environ. Sci.* **2009**, *2*, 1302.
(14) Gubbala, S.; Chakrapani, V.; Kumar, V.; Sunkara, M. K. *Adv. Funct. Mater.* **2008**, *18*, 2411.
(15) Osa, T.; Fujihira, M. *Nature* **1976**, *264*, 349.
(16) Fungo, F.; Otero, L.; Durantini, E. N.; Silber, J. J.; Sereno, L. E. *J. Phys. Chem. B* **2000**, *104*, 7644.
(17) Kay, A.; Gratzel, M. *Chem. Mater.* **2002**, *14*, 2930.
(18) Hawn, D. D.; Armstrong, N. R. *J. Phys. Chem.* **1978**, *82*, 1288.
(19) Sunkara, M. K.; Pendyala, C.; Cummins, D.; Meduri, P.; Jasinski, J.; Kumar, V.; Russell, H. B.; Clark, E. L.; Kim, J. H. *J. Phys. D: Appl. Phys.* **2011**, *44*, 173032.
(20) Batzill, M.; Diebol, U. *Prog. Surf. Sci.* **2005**, *79*, 47.
(21) Park, N. G.; Kang, M. G.; Ryu, K. S.; Kim, K. M.; Chang, S. H. *J. Photochem. Photobiol. A-Chem.* **2004**, *161*, 105.
(22) Ford, W. E.; Rodgers, M. A. J. *J. Phys. Chem.* **1994**, *98*, 3822.
(23) Ford, W. E.; Wessels, J. M.; Rodgers, M. A. J. *J. Phys. Chem. B* **1997**, *101*, 7435.
(24) Sanjinés, R.; Demarne, V.; Lévy, F. *Thin Solid Films* **1990**, *193*, 935.
(25) Korotkov, R. Y.; Farran, A. J. E.; Culp, T.; Russo, D.; Roger, C. *J. Appl. Phys.* **2004**, *96*, 6445.
(26) Könenkamp, R. *Phys. Rev. B* **2000**, *61*, 11057.
(27) Wang, Y. F.; Li, J. W.; Hou, Y. F.; Yu, X. Y.; Su, C. Y.; Kuang, D. B. *Chem.—Eur. J.* **2010**, *16*, 8620.
(28) Houarner-Rassin, C.; Chaignon, F.; She, C.; Stockwell, D.; Blart, E.; Buvat, P.; Lian, T.; Odobel, F. *Photochem. Photobiol., A* **2007**, *192*, 56.
(29) Audebert, P.; Sadki, S.; Miomandre, F.; Lanneau, G.; Frantz, R.; Durand, J. O. *J. Mater. Chem.* **2002**, *12*, 1099.
(30) Frantz, R.; Durand, J.-O.; Lanneau, G. F.; Jumas, J. C.; Olivier-Fourcade, J.; Cretin, M.; Persin, M. *Eur. J. Inorg. Chem.* **2002**, 1088.
(31) Ryan, M. A.; Spitler, M. T. *Langmuir* **1988**, *4*, 861.
(32) Plass, K. E.; Liu, X. L.; Brunschwig, B. S.; Lewis, N. S. *Chem. Mater.* **2008**, *20*, 2228.
(33) Rohde, R. D.; Agnew, H. D.; Yeo, W. S.; Bailey, R. C.; Heath, J. R. *J. Am. Chem. Soc.* **2006**, *128*, 9518.
(34) Marrani, A. G.; Cattaruzza, F.; Decker, F.; Zanoni, R.; Cossi, M.; Iozzi, M. F. *J. Nanosci. Nanotechnol.* **2010**, *10*, 2901.
(35) Das, M. R.; Wang, M.; Szunerits, S.; Gengembre, L.; Boukherroub, R. *Chem. Commun.* **2009**, 2753.
(36) Ruther, R. E.; Rigsby, M. L.; Gerken, J. B.; Hogendoorn, S. R.; Landis, E. C.; Stahl, S. S.; Hamers, R. J. *J. Am. Chem. Soc.* **2011**, *133*, 5692.

(37) Devadoss, A.; Chidsey, C. E. D. *J. Am. Chem. Soc.* **2007**, *129*, 5370.
(38) Devaraj, N. K.; Decreau, R. A.; Ebina, W.; Collman, J. P.; Chidsey, C. E. D. *J. Phys. Chem. B* **2006**, *110*, 15955.
(39) Kolb, H. C.; Finn, M. G.; Sharpless, K. B. *Angew. Chem., Int. Ed.* **2001**, *40*, 2004.
(40) Hein, J. E.; Fokin, V. V. *Chem. Soc. Rev.* **2010**, *39*, 1302.
(41) Rostovtsev, V. V.; Green, L. G.; Fokin, V. V.; Sharpless, K. B. *Angew. Chem.-Int. Edit.* **2002**, *41*, 2596.
(42) Collman, J. P.; Devaraj, N. K.; Chidsey, C. E. D. *Langmuir* **2004**, *20*, 1051.
(43) Landis, E. C.; Hamers, R. J. *Chem. Mater.* **2009**, *21*, 724.
(44) Tan, E. T. H.; Ho, G. W.; Wong, A. S. W.; Kawi, S.; Wee, A. T. S. *Nanotechnology* **2008**, *19*, 255706.
(45) Ito, S.; Murakami, T. N.; Comte, P.; Liska, P.; Grätzel, C.; Nazeeruddin, M. K.; Grätzel, M. *Thin Solid Films* **2008**, *516*, 4613.
(46) Ziessel, R.; Grosshenny, V.; Hissler, M.; Stroh, C. *Inorg. Chem.* **2004**, *43*, 4262.
(47) Shirley, D. A. *Phys Rev. B* **1972**, *5*, 4709.
(48) Conny, J. M.; Powell, C. J. *Surf. Interface Anal.* **2000**, *29*, 856.
(49) Mora-Seró, I.; Dittrich, T.; Garcia-Belmonte, G.; Bisquert, J. *J. Appl. Phys.* **2006**, *100*, 103705.
(50) Anta, J. A.; Mora-Seró, I.; Dittrich, T.; Bisquert, J. *J. Phys. Chem. C* **2007**, *111*, 13997.
(51) Kronik, L.; Leibovitch, M.; Fefer, E.; Burstein, L.; Shapira, Y. *J. Electron. Mater.* **1995**, *24*, 379.
(52) Franking, R. A.; Landis, E. C.; Hamers, R. J. *Langmuir* **2009**, *25*, 10676.
(53) Hamers, R. J.; Chambers, S. A.; Evans, P. E.; Franking, R.; Gerbec, Z.; Gopalan, P.; Kim, H.; Landis, E. C.; Li, B.; McCoy, M. W.; Ohsawa, T.; Ruther, R. E. *Phys. Status Solidi C* **2010**, *7*, 200.
(54) Li, B.; Franking, R.; Landis, E. C.; Kim, H.; Hamers, R. J. *ACS Appl. Mater. Interfaces* **2009**, *1*, 1013.
(55) Shishkov, I. F.; Geise, H. J.; Van Alsenoy, C.; Khristenko, L. V.; Vilkov, L. V.; Senyavian, V. M.; Van der Veken, B.; Herrebout, W.; Lokshin, B. V.; Garkusha, O. G. *J. Mol. Struct.* **2001**, *567*, 339.
(56) Amalric-Popescu, D.; Bozon-Verduraz, F. *Catal. Today* **2001**, *70*, 139.
(57) Wagner, C. D.; Naumkin, A. V.; Kraut-Vass, A.; Allison, J. W.; Powell, C. J.; Rumble, J. R., Jr. *NIST X-ray Photoelectron Spectroscopy Database*, version 3.5; National Institute of Standards and Technology: Gaithersburg, MD, 2003.
(58) Moulder, J. F.; Stickle, W. F.; Sobol, P. E.; Bomben, K. D. *Handbook of X-ray Photoelectron Spectroscopy*; Perkin-Elmer Corporation: Eden Prairie, MN, 1992.
(59) Collman, J. P.; Devaraj, N. K.; Eberspacher, T. P. A.; Chidsey, C. E. D. *Langmuir* **2006**, *22*, 2457.
(60) Popenoe, D. D.; Deinhammer, R. S.; Porter, M. D. *Langmuir* **1992**, *8*, 2521.
(61) Laviron, E. J. *Electroanal. Chem.* **1979**, *101*, 19.
(62) Murray, R. W. In *Electroanalytical Chemistry Vol. 13: Chemically Modified Electrodes*; Bard, A. J., Ed.; Marcel Dekker: New York, 1984; p 191.
(63) Bisquert, J.; Zaban, A.; Salvador, P. *J. Phys. Chem. B* **2002**, *106*, 8774.
(64) Fabregat-Santiago, F.; Mora-Seró, I.; Garcia-Belmonte, G.; Bisquert, J. *J. Phys. Chem. B* **2003**, *107*, 758.
(65) Kim, H.; Laitinen, H. A. *J. Electrochem. Soc.* **1975**, *122*, 53.
(66) Creager, S. E.; Rowe, G. K. *Anal. Chim. Acta* **1991**, *246*, 233.
(67) Campagna, S.; Puntoriero, F.; Nastasi, F.; Bergamini, G.; Balzani, V. in *Photochemistry and Photophysics of Coordination Compounds I*; Springer-Verlag Berlin: Berlin, 2007; Vol. 280, p 117.
(68) Jakubikova, E.; Chen, W. Z.; Dattelbaum, D. M.; Rein, F. N.; Rocha, R. C.; Martin, R. L.; Batista, E. R. *Inorg. Chem.* **2009**, *48*, 10720.
(69) Sauvage, J. P.; Collin, J. P.; Chambron, J. C.; Guillerez, S.; Coudret, C.; Balzani, V.; Barigelletti, F.; De Cola, L.; Flamigni, L. *Chem. Rev.* **1994**, *94*, 993.
(70) Winkler, J. R.; Netzel, T. L.; Creutz, C.; Sutin, N. *J. Am. Chem. Soc.* **1987**, *109*, 2381.
(71) Anne, A.; Demaille, C. *J. Am. Chem. Soc.* **2006**, *128*, 542.
(72) Anne, A.; Demaille, C. *J. Am. Chem. Soc.* **2008**, *130*, 9812.
(73) Uzawa, T.; Cheng, R. R.; White, R. J.; Makarov, D. E.; Plaxco, K. W. *J. Am. Chem. Soc.* **2010**, *132*, 16120.
(74) Landis, E. C.; Klein, K. L.; Liao, A.; Pop, E.; Hensley, D. K.; Melechko, A. V.; Hamers, R. J. *Chem. Mater.* **2010**, *22*, 2357.
(75) Fan, C. H.; Plaxco, K. W.; Heeger, A. J. *Proc. Natl. Acad. Sci. U.S. A.* **2003**, *100*, 9134.
(76) Beratan, D. N.; Onuchic, J. N.; Hopfield, J. J. *J. Chem. Phys.* **1987**, *86*, 4488.